urations. The black circles are the results of calculating the $\langle l_s \rangle$ values obtained by using Monte Carlo simulations by the method explained in section II. Consider a short chain of three beads as in Figure 1c. Bead number 3 in Figure 1c can be involved in four positions, forming a kink, and in one position forming a straight line. Thus according to eq 1, averaging over the five possible configurations for a chain of three beads, we obtain $\langle l_s \rangle = (4 \times 1 + 1 \times 2)/5 = 6/5 = 1.2$. Similar calculations for $N = 4$ (25 possible configurations) result in $\langle l_s \rangle = 1.24$, and for $N = 5$ (121 configurations), $\langle l_s \rangle = 1.256$. The exact results, together with the Monte Carlo results, for chains of $N = 8, 10, 12, ..., 32$ and for $N = 40, 48$, and 64 are described in Figure 14.

It is interesting to observe the increase in the resulting values of $\langle l_s \rangle$ with N and to analyze it in terms of the limitations that are added to the chains due to the addition of beads. For $N = 2$ the value of $\langle l_s \rangle$ equals 1. In the transition from $N = 2$ to $N = 3$, the excluded volume limitation is added; i.e., the possibility of turning opposite to the previous vector is blocked. This limitation, together with the straight configuration (in Figure 1c with bead number 3 at site 3''), change the corresponding $\langle l_s \rangle$ value drastically from 1 to 1.2. For $N = 4$, the increase in $\langle l_s \rangle$ due to the straight configuration is now smaller because its weight has decreased between the 25 configurations resulting in $\langle l_s \rangle = 1.24$. For $N = 5$, an additional limitation enters: the fifth bead is prevented not only from choosing an opposite vector but also from occupying the place of the bead at the origin. The increase in $\langle l_s \rangle$ continues until the additional length from the only straight configuration is negligible in proportion to the number of configurations available, and the value of $\langle l_s \rangle$ converges to a constant value as can be seen from Figure 14. Thus, the resulting value of $\langle l_s \rangle$ for self-avoiding walk chains of $N \geq 30$ seems to be independent of N.

References and Notes

(1) Flory, P. J. *Statistical Mechanics of Chain Molecules*; Wiley: New York, 1969.
(2) Yamakawa, H. *Modern Theory of Polymer Solutions*; Harper and Row: New York, 1971.
(3) Odijk, T. *J. Polym. Sci.* **1977**, *15*, 477.
(4) Skolnick, J.; Fixman, M. *Macromolecules* **1977**, *10*, 944.
(5) De Gennes, P. G. *Scaling Concepts in Polymer Physics*; Cornell University Press: Ithaca, NY, 1979.
(6) Le Bret, M. *J. Chem. Phys.* **1982**, *76*, 6243.
(7) Fixman, M. *J. Chem. Phys.* **1982**, *76*, 6346.
(8) Baumgärtner, A., private communication.
(9) Carnie, S. L.; Christos, G. A. *J. Chem. Phys.* **1988**, *89*, 6484.
(10) (a) Reed, C. E.; Reed, W. F. *J. Chem. Phys.* **1990**, *92*, 6916. (b) Li, X.; Reed, W. F. *J. Chem. Phys.* **1991**, *94*, 4568.
(11) Wattenbager, M. R.; Chan, H. S.; Evans, D. F.; Bloomfield, V. A.; Dill, K. A. *J. Chem. Phys.* **1990**, *93*, 8343.
(12) Hooper, H. H.; Blanch, H. W.; Praunsnitz, J. M. *Macromolecules* **1990**, *23*, 4820.
(13) Brender, C. *J. Chem. Phys.* **1990**, *92*, 4468.
(14) Brender, C.; Lax, M.; Windwer, S. *J. Chem. Phys.* **1981**, *74*, 2576.
(15) Brender, C.; Lax, M.; Windwer, S. *J. Chem. Phys.* **1984**, *80*, 886.
(16) Card, D. N.; Valleau, J. P. *J. Chem. Phys.* **1972**, *52*, 6232.
(17) Shaw J. N. Monte Carlo Calculations for a System of Hard-Sphere Ions: Ph.D. Dissertation, Duke University, NC, 1963.
(18) Brender, C. *J. Chem. Phys.* **1991**, *94*, 3213.
(19) Ma, S. K. *Modern Theory of Critical Phenomena*; Benjamin: Reading, MA, 1976.
(20) Brender, C. *J. Chem. Phys.* **1990**, *93*, 2736.
(21) Christos, G. A.; Carnie, S. L. *J. Chem. Phys.* **1990**, *92*, 7661.
(22) Barber, M. N. In *Phase Transition and Critical Phenomena*; Domb, C., Lebowitz, J., Eds.; Academic: London, 1983; Vol. 8.
(23) Barrow, G. M. *Introduction to Molecular Spectroscopy*; McGraw-Hill: New York, 1962.
(24) Patel, G. N.; Chance, R. R.; Witt, J. D. *J. Chem. Phys.* **1979**, *70*, 4387.
(25) Aime, J. P.; Bargain, F.; Fave, J. L., Rawiso, M.; Schott, M. *J. Chem. Phys.* **1988**, *89*, 6477.
(26) Viallat, A.; Rossi, G. *J. Chem. Phys.* **1990**, *92*, 4548.
(27) Viallat, A. *J. Chem. Phys.* **1990**, *92*, 4557.
(28) Rossi, G. *J. Chem. Phys.* **1991**, *94*, 4031.
(29) Reed, C.; Reed, W. *J. Chem. Phys.* **1991**, *94*, 8479.
(30) Stanley, H. E. In *Fractals and Disordered Systems*; Bunde, A., Havlin, S., Eds.; Springer-Verlag: Berlin, 1991.
(31) Brender, C.; Danino, M. *J. Chem. Phys.*, in press.

Dielectric Relaxation in a Protein Matrix

Daniel W. Pierce and Steven G. Boxer*

Department of Chemistry, Stanford University, Stanford, California 94305-5080
(Received: December 13, 1991)

We report measurements of time-dependent solvation in a protein medium by the fluorescence dynamic Stokes shift method. Picosecond time-correlated single photon counting fluorescence decays on the complex formed by sperm whale apomyoglobin (apoMb) and 2'-(*N*,*N*-dimethylamino)-6-naphthoyl-4-*trans*-cyclohexanoic acid (DANCA) at temperatures between 298 and 243 K show that the decay of the mean emission energy is extremely nonexponential with components spanning and probably exceeding the experimentally observable (20 ps to 20 ns) range. At all temperatures, the observed relaxation is approximately 700 cm^{-1}, but the emission energy at short and long times increases with decreasing temperature. Decays on the low-energy side of the emission band show rise times clearly resolved from the instrument response and rule out a model in which the observed shift results solely from heterogeneity in the population of dye–apoMb complexes. These results suggest that either the activation energies of the rate-limiting motions in the relaxation are dependent on conformational substate, or different types of protein motions with different characteristic frequencies participate in the relaxation. The rate distributions of correlation functions constructed from the data were obtained by maximum entropy fitting and demonstrate the distributed nature of the decay. Free energy perturbation calculations of protein energetics and simulations of electron transfer in proteins introduce a perturbation in a dynamics simulation similar to that created experimentally here. The nanosecond time scale relaxations observed indicate a possible shortcoming of simulations which typically extend at most to 100 ps. Possible relaxations on a much shorter time scale are discussed.

The rates of electron-transfer reactions depend, among other factors, on fluctuations in the energies of the states involved. In condensed-phase reactions, the dynamics of electrostatic interactions with the medium make a significant contribution to such fluctuations and can determine the overall electron transfer rate.[1-5] For many simple solvents the characteristic time for fluctuations is on the order of picoseconds; however, the time scale and magnitude of the dielectric fluctuations relevant to electron transfer in organized media such as in biological systems are less well characterized. A substantial theoretical effort has been directed

* Author to whom correspondence should be addressed.

0022-3654/92/2096-5560$03.00/0

toward obtaining information on the static dielectric properties of proteins,[6-8] and dynamics simulations have been performed in photosynthetic reaction centers to evaluate the contribution of dielectric fluctuations to electron-transfer rates.[9] Experimental information on static properties has recently become available through site-directed mutagenesis.[10-12] Mutants offer the opportunity to dissect the contributions of individual amino acid residues to both static and dynamic dielectric properties.

The time dependence of the Stokes shift of a fluorescent molecule offers a useful experimental technique for obtaining information on dielectric relaxation phenomena and has been widely used to study simple solvents.[13-27] An appropriate probe molecule has the following characteristics:[28] (i) it should have a large change in dipole moment between the ground and excited states so that relatively large reorganizations can be observed; (ii) it should not participate in excited-state interactions (e.g., proton transfers, exciplex formation) other than the one of interest; (iii) it should have a fluorescence lifetime similar to that of the process to be measured; (iv) it should be excited directly to the emitting electronic state so that the data are not contaminated by electronic relaxation in the probe molecule which may be medium dependent; and (v) for studies in a protein the probe molecule should bind with high affinity, and the complex should be structurally characterizable.

Complexes between various dye molecules and apomyoglobin (apoMb,[29] Mb where the native heme group has been removed) have been investigated for many years.[30] For certain dyes it has been shown that a 1:1 complex between the dye and apoMb is formed and that the dye occupies the heme binding site as evidenced by dissociation of the dye upon addition of heme. Early nanosecond time-dependent studies by Brand and co-workers using the probe molecule *N*-(*p*-tolyl)-2-aminonaphthalene-6-sulfonate (TNS) showed that there were significant relaxations on the nanosecond time scale and suggested faster processes may occur as well.[31] Frequency domain measurements have confirmed these observations.[32,33] We report here time domain measurements on the picosecond time scale for the complex between 2′-(*N*,*N*-dimethylamino)-6-naphthoyl-4-*trans*-cyclohexanoic acid (DANCA)[28] and sperm whale apoMb. Dielectric relaxation has been measured in glycerol using this probe.[34] This system has many, if not all, of the characteristics listed above. DANCA binds to apoMb with moderate affinity (K_D = 12 μM). The dipole moments of DANCA in the ground and excited state are collinear and have been estimated as 2 and 20 D, respectively.[35] The emitting state can be excited directly.[36] The 3.5-ns fluorescence lifetime enables observation of excited-state processes from the 20-ps instrument limit of this study until about 20 ns. To date no complex between a dye and apoMb has been characterized by X-ray crystallography; two-dimensional NMR experiments on the DANCA–apoMb complex are underway in our laboratory. Recent results using a deuterium–hydrogen exchange method suggest that the dye is bound inside the heme pocket.[37] While this work was in progress, a brief report on a different apoMb–dye complex was published.[38] The results are quite different from those we have obtained, and it is likely that some of the differences are related to properties of the dye or the complex.

Experimental Procedures

DANCA was generously provided by F. Farris and Professor Gregorio Weber at the University of Illinois who initially characterized its complex with apoMb.[28] Sperm whale Mb was obtained from Sigma (Type II) and was used without further purification. ApoMb was prepared by a method modified from that of Teale.[39] A 75-mg portion Mb was dissolved in 2 mL of H_2O. The pH was lowered to 2.0–2.4 with 0.5 M HCl on ice, and the sample extracted three times with several volumes of cold 2-butanone. This solution was immediately loaded onto a Pharmacia PD-10 prepacked G-25 column equilibrated with water. The pH of the eluted protein was adjusted to 4.7–5.2 with 0.5 M NaOH and the volume reduced to less than 2 mL in a Centricon-10 (Amicon). The concentrate was then run over another PD-10 column, the pH of the eluate adjusted to 6.3, and the volume reduced until the desired concentration was obtained. The apoMb and DANCA concentrations were determined optically at 280 nm (ϵ = 15 700) and 363 nm (ϵ = 8700), respectively. DANCA purity was determined by comparing the absorbance at 308 and 363 nm. Samples with A_{363}/A_{308} less than 2.55 were rejected.[40] No buffer was employed, as apoMb aggregates more rapidly in the presence of salts.[41] The pH of the solutions was stable due to self-buffering by the apoMb. Steady-state front-face fluorescence spectra were recorded on a Spex Fluorolog fluorimeter using the same sample holder described below for time-resolved measurements and were corrected for lamp instabilities and the wavelength-dependent response of the detection optics and photomultiplier. The same (9 nm) emission bandpass was employed as for the transient measurements described below.

Samples in water contained 2.0 mM apoMb and 57 μM DANCA. Samples in 50% gly/H_2O contained 1.0 mM apoMb and 57 μM DANCA. With K_D = 12 μM, these concentrations correspond to free DANCA proportions of 0.6 and 1.3%, respectively. Experimentally, the lack of detectable emission from free DANCA was verified by measuring the excitation-wavelength dependence of the emission spectrum. The ratio of the extinction coefficients of free and bound DANCA changes from 0.789 to 1.23 from 375 to 320 nm, or a factor of 1.56. The emission maximum of free DANCA occurs at 520 nm, well out on the red side of the bound DANCA spectrum. For identical dye absorption cross sections, the emission of free DANCA to the red of 520 nm is about 4 times as intense as the emission of bound DANCA. A typical S/N ratio for this region is 100, so a free DANCA proportion of $1/(4 \times 0.56 \times 100) = 0.5\%$ would cause an observable change in the line shape. All samples were checked in this manner before and after data collection. Samples with detectable line-shape changes were not used.

For time-resolved measurements, the excitation light source was a YAG-pumped, cavity-dumped dye laser using DCM dye operating at 800 kHz and 690 nm. The 20-ps pulses were frequency doubled and the remaining 690-nm light was removed before the sample. Samples consisted of 30–100 μL of DANCA–apoMb solution in a 1-mm quartz cuvette. The temperature was controlled to within 0.5 °C using a home-built sample holder equipped with thermoelectric coolers. Emitted light was collected and focused on a polarizer at the entrance slit of a subtractive dispersion monochromator and detected at the magic angle with a microchannel plate and time-correlated single photon counting electronics. The overall instrument response was measured from the scattering off the sample or a ground glass surface and was 50 ps. Decays were taken at 12 or 24 wavelengths in 16- or 8-nm increments between 376 and 568 nm. The bandpass of the monochromator was 9 nm. Decays taken with a 9- or 4.5-nm bandpass at several wavelengths were indistinguishable. Approximately 45 min were required to collect a typical decay which contained about 4×10^6 counts dispersed over 4096 channels with a peak intensity of about 3.3×10^4 counts and a dwell time of 8 ps per channel. As discussed above, the steady-state fluorescence spectrum was monitored frequently to evaluate sample quality. At room temperature, it was necessary to replace the samples about once a day. At lower temperatures, samples were stable for several days. The change in samples at room temperature did not depend on illumination conditions and is probably the result of slow aggregation of the apoMb.

Results and Methods of Analysis

Figure 1 shows fluorescence decays measured at several wavelengths in the DANCA emission band at room temperature. The decays are highly nonexponential, and slow progressively as the detection wavelength is scanned from the high-energy to the low-energy side of the emission band. Each decay was deconvolved from the instrument response function using an iterative nonlinear least-squares convolve-and-compare procedure based on the Marquardt algorithm using software developed in this laboratory. An arbitrary number of exponential decays were convolved with the instrument response to give a model for the experimental decay. We emphasize that no physical significance is attached to these

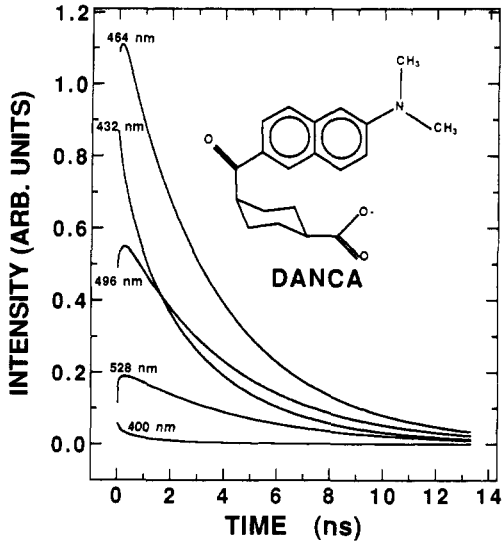

Figure 1. Deconvolved fluorescence decays of the DANCA–apoMb complex from 400 to 528 nm in 32-nm increments at 298 K. The area under each trace has been scaled to the steady-state spectrum amplitude at the appropriate wavelength. Note the resolved rises for the three decays at lower energies. The inset shows the structure of DANCA. No implications as to the conformation of DANCA are intended. The ground- and excited-state dipoles form between the amino nitrogen and the keto oxygen. The cyclohexyl propionate moiety improves the affinity of DANCA for apoMb but does not affect the properties of the chromophore.[28]

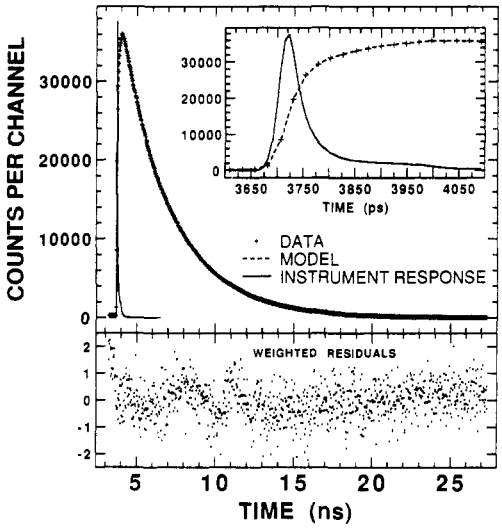

Figure 2. Typical raw data at 440 nm and 298 K with a five-exponential convolved fit. This fitting form is used only to provide a computationally convenient model function for the deconvolution. The components in the fit have no physical meaning. The raw data and fit have been reduced with a three-point average for plotting, so the dwell time per channel pictured is 24 instead of 8 ps as the data were collected. The instrument response is scaled down to the same peak height as the decay. The inset shows the same data on an expanded scale. The lower panel shows the residuals divided by the square root of the signal, appropriate for Poisson distributed noise.

exponentials, and that this functional form is used for computational convenience in the deconvolution. Amplitudes were not restricted to positive values. Five components were necessary in most cases to obtain a good fit with random residuals (see Figure 2). The convolution algorithm was adapted from a centered δ-pulse algorithm.[42]

The apoMb contained some fluorescent impurities which we were not able to remove. Background fluorescence accounted for less than 1% of the total fluorescence, but up to 30% of the signal at the extremes of the band. Temporally, the background fluorescence occurred on the picosecond to nanosecond time scale and was somewhat faster than the DANCA decay. The deconvolved decays were corrected for background fluorescence from the apoMb by subtracting an appropriately scaled and deconvolved decay obtained from samples containing only apoMb. The apoMb background decay kinetics were found to be very nearly wavelength independent, so decays were not collected at all wavelengths. Decay parameters for missing wavelengths are obtained by combining the parameters from adjacent wavelengths. The corrected decay was then normalized to the similarly corrected steady-state spectrum. The transient spectra shown in Figure 3 were then extracted and fit to a log-normal line-shape function:[22,43]

$$a(\nu) = a_0 \exp\{-\ln(2)[\ln(1 + 2b(\nu - \nu_p)/\Delta)/b]^2\}, \quad \text{for } \alpha > -1$$

$$= 0 \quad \text{for } \alpha \leq -1$$

where ν_p is the peak position of the band and $\alpha = 2b(\nu - \nu_p)/\Delta$. The numerical first moment of this fit plotted as a function of time is shown in Figure 4. When twice as many wavelengths were employed in the analysis of the 298 K data (8-nm increments), the decay of the mean emission had a slightly larger overall amplitude (850 vs 824 cm^{-1}) and a nearly identical shape, indicating that 16-nm increments can be employed without substantial loss in accuracy.

The time dependence of the total fluorescence intensity was calculated as the numerical integral of the log-normal fit. The intensity decay was a single exponential within 2% of the total amplitude for all temperatures, with a $1/e$ time of 3.5 ns. This result indicates that if heterogeneous emission[44] or energy de-

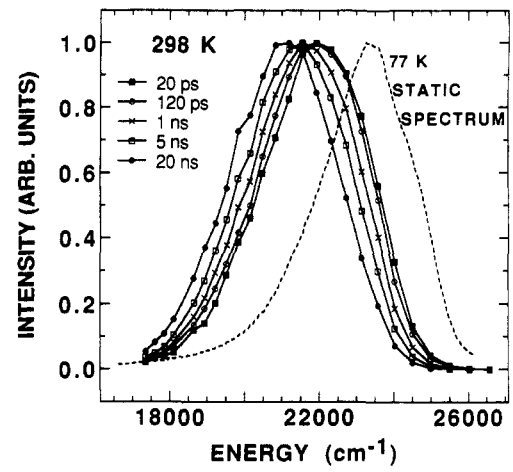

Figure 3. Transient fluorescence spectra extracted from a set of decays at 298 K such as in Figure 1. The spectra have been peak normalized. The static fluorescence spectrum at 77 K is included to indicate where the $t = 0$ spectrum may be located.

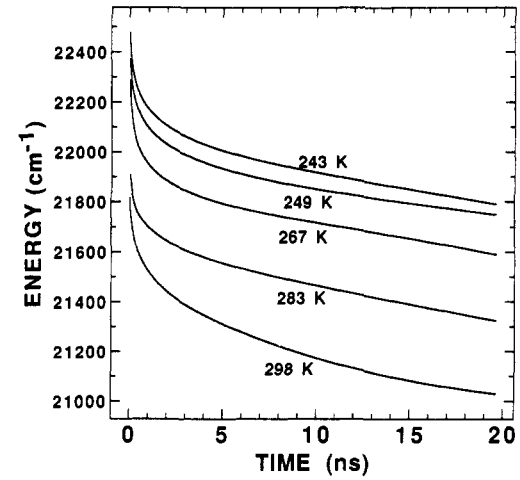

Figure 4. Decay of the numerical mean of the log-normal fit to the transient fluorescence spectra (see Figure 3) at five temperatures. The data at the two highest temperatures are in H_2O, and at the three lower temperatures in 50% glycerol/H_2O. The limits of integration for calculation of the mean were taken as the extreme wavelengths of the data.

TABLE I: Steady-State Emission Parameters of DANCA-APOMB

solvent	temp, K	mean energy,[a] cm^{-1}	fwhm,[a] cm^{-1}
H_2O	308	21 791	3649
H_2O	303	21 834	3567
H_2O	298	21 874	3508
H_2O	283	21 969	3354
50% glycerol/H_2O	308	21 946	3573
50% glycerol/H_2O	303	22 002	3513
50% glycerol/H_2O	298	22 056	3440
50% glycerol/H_2O	283	22 186	3259
50% glycerol/H_2O	267	22 281	3147
50% glycerol/H_2O	249	22 411	3095
50% glycerol/H_2O	243	22 463	3088
50% glycerol/H_2O	77	23 014	3125

[a] These parameters were taken from log-normal fits to the spectra in order to enable comparison with the time-dependent data.

pendence of the radiative rate[45] occurs in this system they constitute a minor effect. On the basis of this lifetime, the data were truncated at 20 ns. The intensity of the fluorescence had decayed to 0.33% of its initial value at this point, or about 110 counts/channel in the raw data. Typical noise backgrounds were 4–30 counts/channel, so the S/N of the data at 20 ns is about $100^{1/2}$ (Poisson distributed noise) for a typical decay. This S/N applies to spectra at 8-ps intervals, so it is quite adequate to track changes occurring on the nanosecond time scale.

In contrast to the result obtained by Macgregor and Weber,[28] we found that the steady-state spectrum at room temperature is perturbed by the addition of glycerol. The spectrum at 308 K in 50% glycerol/H_2O is similar to that in H_2O at 283 K (Table I).

Discussion

1. Evidence for Dielectric Relaxation. Decays on the low-energy side of the emission band rise more slowly than the integral of the instrument response at all the temperatures studied, and the model functions used for deconvolution must contain one or more exponentials with negative amplitudes to successfully fit the data. This is the unambiguous signature of population flux of excited states into configurations which fluoresce at these wavelengths. As the excitation occurs directly into the emitting state, and decays on the high-energy side rise with the instrument response and show a rapid initial decay, one may conclude that population is moving from configurations which fluoresce at higher energy to configurations which fluoresce at lower energy. Given the large $\Delta\mu$ and solvent-dependent emission energy of DANCA,[28] it seems reasonable to assume that dielectric relaxation is the process which causes the population flux. If true, then some, if not all, of the observed time dependence of the mean emission energy must be due to dielectric relaxation.[46] Unlike previous time-domain studies in which either resolved rising edges were not observed[31] or excitation did not occur directly into the emitting state,[38] a model based on heterogeneity of the DANCA–apoMb complexes is not consistent with our results.

2. Room Temperature Results. Figure 5 shows the decay of the mean emission energy at room temperature and fits to several functional forms. It is evident that the decay is not well described by a single exponential, but can be reasonably well fit with three exponentials. The exponential lifetimes are 80 ps, 0.68 ns, and 11.6 ns, with amplitudes of 124, 187, and 605 cm^{-1}, respectively, clearly demonstrating the distributed nature of the decay. Our intent in giving these parameters is not to claim that the decay is triple exponential. Various model functions were also tested including a log-normal distribution of rates, stretched exponential, Γ-distribution of exponentials and a time-dependent rate. Of these, a time-dependent rate gave the best fit. Thus, in contrast to simple solvents, where analogous data gives decays that are often well described by a single exponential, the decay of the average energy in the protein matrix occurs on a considerable range of time scales from tens of picoseconds (the limit of the instrumentation used) to nanoseconds (the limit imposed by the fluorescence lifetime).

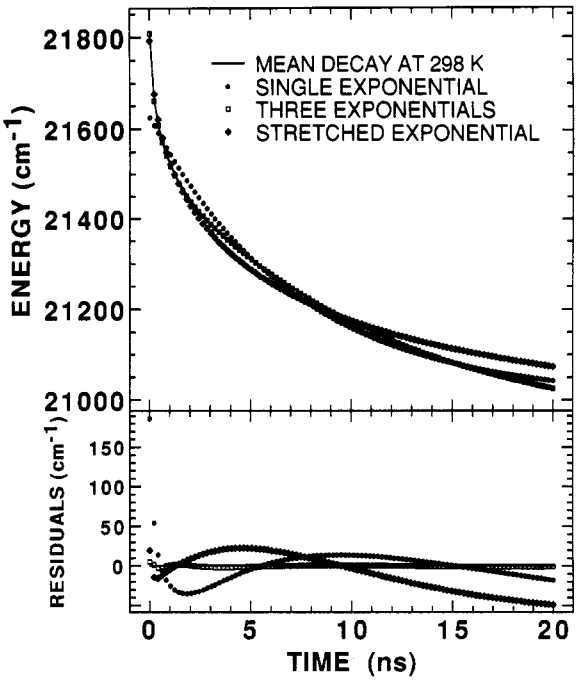

Figure 5. Decay of the mean emission energy at 298 K and fits to a single exponential, three exponentials, and a stretched exponential function $A(t) = A_0 \exp\{-(kt)^\beta\}$, with $\beta = 0.48$.

TABLE II: Emission Energy at Early and Long Times in cm^{-1}

temp, K	20 ps	20 ns	diff (20 ps − 20 ns)
298	21 804	21 009	795
283	21 898	21 306	592
267	22 283	21 584	699
249	22 359	21 745	614
243	22 475	21 786	689

It may well be that further relaxation occurs on a longer time scale; however, this cannot be determined using emission from the singlet state of DANCA.

Singular value decomposition analysis[47] of the data matrix yields basis spectra corresponding to the zeroth, first, and second derivatives of the mean spectrum, consistent with the picture of a band shifting in time. The shift is too large to be represented by a first-derivative component alone, and the second derivative contributes significantly at very early and very long times. The transient spectra reconstituted from these three basis spectra show a mean emission decay with a very similar shape but a slightly smaller (50 cm^{-1}) overall amplitude than the mean decay obtained from the complete data matrix.

It is perhaps not surprising that components of relaxation were observed over the entire range of experimentally accessible time scales. Proteins can undergo motions on time scales from femtoseconds to seconds, and it is reasonable to expect that motions in all modes will contribute to the overall relaxation. Several investigators have suggested that very fast (a few picoseconds or less) solvation may occur in proteins.[48–50] Our experiment does not have sufficient time resolution to directly observe such processes but can serve as a starting point for estimation of their amplitude (see section 5 below). At least in this complex it appears that relaxation occurs over a wide range of time scales. This observation is consistent with a model in which the protein exists in conformational substates with different activation energies for the rate-limiting motion(s) in the relaxation,[51] or with a model in which displacements in protein modes over a wide range of mode frequencies contribute to the relaxation.

3. Temperature Dependence of the Decay. A striking aspect of the data shown in Figure 4 is the approximate temperature independence of the observable relaxation. Over the temperature range investigated, the mean emission energy at the beginning and end of the decay changes by about 700 cm^{-1} and increases with decreasing temperature, while the relaxation during the decay

has an average value of 680 cm^{-1} (see Table II) and no obvious trends with temperature. This result is quite different from that obtained in a simple solvent such as 1-propanol,[22] where the average relaxation time was observed to slow down and by a factor of 23 and increase in amplitude by 30% as the temperature was lowered over a similar range and the viscosity increased by a factor of 10. From 298 to 243 K the viscosity of 50% glycerol/H_2O increases by a factor of 30.[52] Given the large change in bulk solvent viscosity, the lack of dramatic changes in the observed dielectric relaxation would be difficult to explain if the dye were bound to the exterior of the protein or otherwise made significant contact with the external solvent. If the dye is is the interior of the protein, the modest changes imply that the internal motions of the protein and the motions of the solvent surrounding it are weakly coupled.

The observed fluorescence behavior can be explained in terms of two models. In the first, the true value of the mean emission at zero time is independent of temperature, but the amplitude of the relaxation between 0 and 20 ps decreases with decreasing temperature. Similarly, the true value at infinite time is temperature independent, but the amplitude after 20 ns increases with decreasing temperature. Then the effect of changing the temperature is simply to change the portion of the total relaxation curve which lies within the observable time window. Alternatively, the values of the zero and infinite time emission energies (and therefore the structure of the dye–protein complex) may be temperature dependent. In this case, the protein motions which participate in the relaxation must be approximately temperature independent over the range studied.

It is interesting to compare this behavior to that of carbon monoxide (CO) recombination to myoglobin over the same temperature range. In 75% glycerol/H_2O over the same range of temperatures, the viscosity increases by a factor of 100. The bimolecular rate constant decreases from 735[CO] to 137[CO] s^{-1}, the geminate rate constant decreases from 5.8×10^6 to 1.0×10^6 s^{-1}, and the amplitude of the geminate process increases from 10% to more than 83% for human Mb.[53] The observation that all of these recombination parameters change by about the same factor together with the inference of weak coupling between the protein interior and bulk solvent from the fluorescence data suggests that the changes in the geminate and bimolecular CO recombination rates are, to a first approximation, caused by changes in the microscopic rates for CO entering and leaving the protein interior, and that microscopic steps occurring within the protein are less affected by the bulk viscosity.

4. Correlation Function Analysis. If suitable values for the mean emission energies at $t = 0$ and $t = \infty$ can be determined, the decay of the emission energy can be converted into the dimensionless solvent correlation function: $C(t) = [\nu(t) - \nu(\infty)]/[\nu(0) - \nu(\infty)]$. van der Zwan and Hynes derived the result that, in the continuum limit, this correlation function can be identified with the dielectric friction function used to model the effect of solvent fluctuations on an electron-transfer reaction.[54] This important result provides the theoretical basis for relating the Stokes shift dynamics to electron-transfer rates.

An error in the value of $\nu(0)$ will principally affect the amplitude of any unresolvably fast components in the correlation function, and if the function is not constrained to equal unity at $t = 0$, the only effect is an overall scaling factor, so no serious artifacts are introduced by taking $\nu(0)$ as the position of the mean emission at 20 ps. As $\nu(\infty)$ appears in both the numerator and denominator, the shape of the function is affected, and choosing $\nu(\infty)$ as the position of the mean emission at 20 ns would lead to a correlation function with discontinuous first and higher derivatives. When the mean decays are fit to three exponentials with an adjustable baseline, the baseline parameter increases with decreasing temperature in parallel with $\nu(20$ ps) and $\nu(20$ ns). However, the optimum value of this parameter for the fit depends critically on the first and second derivatives of the tail of the decay where the signal becomes small. Therefore, to compare correlation functions for different temperatures, we took $\nu(\infty)$ to be $\nu(20$ ns) $- \Delta$, where Δ is the average energy difference between $\nu(20$ ns) and the baseline of a three-exponential fit. This may have little relation to the real $\nu(\infty)$ but ensures that all the temperatures are treated the same way and that there is some amplitude after 20 ns so that fitting functions can decay smoothly to zero.

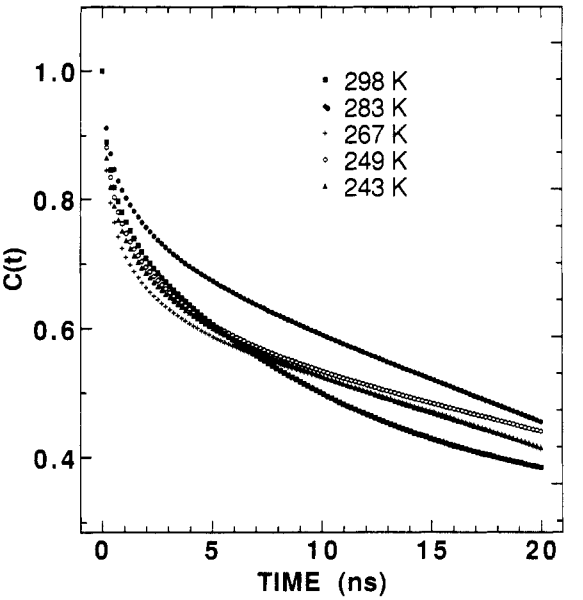

Figure 6. Apparent solvent correlation functions at five temperatures with $\nu(0)$ taken as the energy at $t = 20$ ps, and $\nu(\infty)$ taken as $\nu(20$ ns) $- \Delta$, where Δ is the average energy difference between $\nu(20$ ns) and the baseline of a three-exponential fit.

The correlation functions determined as described above are shown in Figure 6. The main purpose of these functions is to compare the relaxation at different temperatures and to ask what rates are present in the decay. The correlation functions are nonexponential and show no obvious trends with temperature.

The problem of determining what rates are present in the data is the problem of inverting the Laplace transform of the rate distribution, and is notoriously ill-conditioned.[55] The problem is to select from the family of distributions which fit the data to within the errors that distribution which contains only features necessary to fit the data, and no spurious features. A means of finding this distribution is provided by the maximum entropy method.[51,55-57] In this application the distribution consists of a set of exponential rates at equal intervals in log (rate) space, with equal starting amplitudes such that the total amplitude is 1. The algorithm adjusts the amplitudes to obtain a reasonable value of χ^2 [57] while simultaneously maximizing an entropy term $S = \sum f_i \ln (f_i)$, where the f_i's are the normalized amplitudes. The entropy term drives the solution to the distribution which is least correlated (i.e., has the fewest features and smoothest behavior).

Maximum entropy fitting of the correlation functions using the algorithm described by Skilling and Bryan[57] produces rate distributions that contain a minimum of three features at all temperatures (Figure 7), consistent with the observation that three exponentials fit the mean decays better than unimodal functions such as Gaussian or log-normal rate distributions. The amplitudes do not go to zero on either side of the distribution, indicating that there are fast and slow components which are near the borders of the experimentally accesible range of rates. Maximum entropy will only produce δ-function rate distributions if the signal-to-noise of the data is infinite, and the widths of the observed features depend on how the errors are estimated. The maximum entropy fits are better than the three-exponential fits, so either there are more features present and the signal-to-noise is not adequate to resolve them or one or more of the features is a distributed process with a finite width.

The shape of the correlation function and rate distribution at 298 K is different from that at lower temperatures. More of the amplitude is concentrated in the middle part of the rate distribution and less on the slow end, which may reflect an increase in the rate constant of a slow ($k \simeq 10^7 s^{-1}$) process. The distributions for

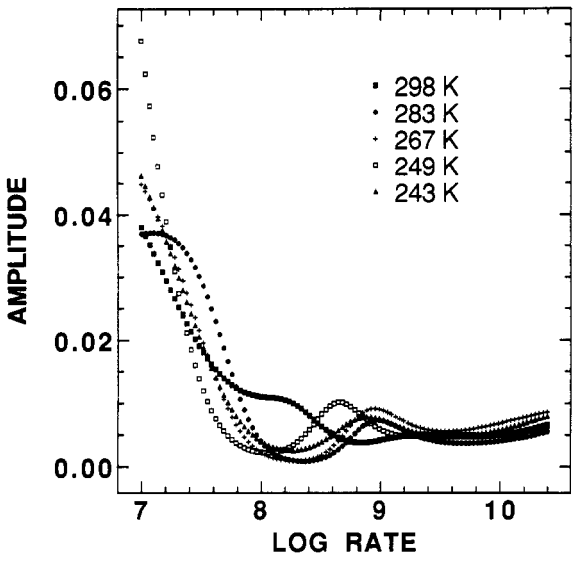

Figure 7. Maximum entropy rate distributions obtained from the correlation functions in Figure 6. Gaussian noise with 1×10^{-3} rms amplitude was added before fitting.

the four lower temperatures do not change in a regular manner as a function of temperature.

Our results differ from those of Bashkin et al.,[38] who reported that the relaxation could be represented by a single 9.1-ns lifetime. We obtain correlation functions which are not single exponential and contain much faster and slower components. The difference at early times may be due to the presence of the convolution artifact in their data. It is difficult to compare the longer time behavior as the lifetime of the slowest component is sensitive to the choice of $\nu(\infty)$. As with our data, the relaxation was not complete at the longest time for which the mean emission could reliably be measured, but no indication was given of how $\nu(\infty)$ was chosen.

5. Relevance to Computer Simulations of Proteins and Ultrafast Solvation. Computer simulations of electron-transfer reactions in proteins[48-50] and free energy perturbation studies of protein energetics[58] both require calculation of the response of the protein to a sudden perturbation. For electron-transfer simulations, the perturbation is the instantaneous change in net charge on the redox active components in the system that occurs when the electron moves. For free energy perturbation studies the system is mutated to the system with which comparison is desired in a series of sudden steps, and the response of the system is simulated after each step. In both cases the response is obtained by molecular dynamics simulations, with the equilibrium free energy of system taken to be the average value over the last few picoseconds of the simulation. Simulations are typically run for 10 ps to at most 100 ps.

The perturbation introduced in our experiment is a sudden ($<10^{-15}$ s) change in the local electric field in the protein and is highly analogous to that introduced in electron-transfer simulations and free energy perturbation studies involving charged or dipolar species. It stands to reason that the response of the systems should be similar. As we and others[31-33,38,59,60] have observed that relaxations occur out to 20 ns and probably longer (at least in this and similar systems), it may be inaccurate to treat properties after a 10- or 100-ps simulation as representing equilibrium in proteins. However, it is likely that this experiment does not resolve the fastest processes present. If $\nu(t)$ has already decayed most of the way to its equilibrium value at 20 ps, then the longer time scale relaxations observed will be proportionately less important.

This brings up the question of how much amplitude in $\nu(t)$ could have been missed. Clearly, it would be desirable to make measurements on a faster time scale to answer this question directly. The recent experimental observation of a substantial (~80%) inertial component to relaxation on the 100-fs time scale in acetonitrile[61] suggests that at least in simple solvents subpicosecond dynamics are critical. We can obtain estimates of the missing amplitude on the basis of static fluorescence energies in nonpolar solvents and in the complex at 77 K. The mean absorption and emission energies of the fluorophore PRODAN (6-propionyl-2-(*N*,*N*-dimethylamino)naphthalene) in cyclohexane at room temperature are 29 326 and 24 506 cm^{-1}, respectively.[28] This molecule contains the same chromophore as DANCA and has an identical fluorescence spectrum in solvents in which both are soluble. This Stokes shift of 4820 cm^{-1} occurs in the absence of dipolar relaxation. A log-normal fit to the room temperature absorption spectrum of the complex yields a mean energy of 27 285 cm^{-1}, compared with the fluorescence energy at 20 ps of 21 804 cm^{-1}. This shift of 5481 cm^{-1} is 661 cm^{-1} larger than the shift observed in cyclohexane and gives an estimate of the missing amplitude at room temperature. Another estimate is obtained by comparing the fluorescence energy at 20 ps with the static spectrum at 77 K. If the motions involved in the relaxation are strongly enough activated that they are effectively frozen at 77 K and the fluorescence spectrum does not depend on temperature in any way not accounted for by temperature-dependent relaxation, then the 77 K spectrum would be identical to the $t = 0$ spectrum. Under these assumptions, our experiment missed approximately 540 cm^{-1} of relaxation at 243 K and 1210 cm^{-1} at 298 K. These energies are comparable to the total shift observed between 20 ps and 20 ns. If the assumption of no relaxation at 77 K is incorrect, then these energies are lower limits to the missing amplitude. One simulation in photosynthetic reaction centers indicated substantial relaxation may occur even at 10 K.[50]

Conclusion

The basic result of this experiment is that a highly nonexponential large amplitude relaxation event occurs in the complex studied between 20 ps and 20 ns after the excitation pulse. The time-resolved rise in amplitude on the low-energy side of the band implies that a process which moves population from one configuration to another is occurring. Given the large $\Delta\mu$ (18 D) of this probe molecule, it is reasonable to assume that dielectric relaxation accounts for some, if not all, of the amplitude. If this is the case, then the solvation dynamics in the complex are very different from what is observed in simple solvents.

Acknowledgment. We thank Drs. F. Farris and Gregorio Weber for a generous amount of DANCA, Peter Steinbach for initial helpful discussions about the maximum entropy method subroutine, Alan Stein for assistance with the transient fluorescence system which was made available through the Center for Materials Research at Stanford, Enrico Gratton for useful discussions about the data, and David Lambright for advice and assistance with the nonlinear least squares, singular value decomposition, and maximum entropy analyses used in this work. This work was supported in part by NIH grant GM27738. D.W.P was supported by an NSF predoctoral fellowship.

References and Notes

(1) Kosower, E. M.; Huppert, D. *Chem. Phys. Lett.* **1983**, *96*(4), 433.
(2) Kosower, E. M.; Kanety, H.; Dodiuk, H.; Striker, G.; Jovin, T.; Boni, H.; Huppert, D. *J. Phys. Chem.* **1983**, *87*, 2479.
(3) Kosower, E. M.; Kanety, H. *J. Am. Chem. Soc.* **1983**, *105*, 6236.
(4) Kosower, E. M.; Huppert, D. *Annu. Rev. Phys. Chem.* **1986**, *37*, 127.
(5) Hwang, J.-K.; Creighton, S.; King, D.; Whitney, D.; Warshel, A. *J. Chem. Phys.* **1988**, *89*(2), 859.
(6) Matthew, J. B. *Annu. Rev. Biophys. Chem.* **1985**, *14*, 387.
(7) Sharp, K. A.; Honig, B. *Annu. Rev. Biophys. Biophys. Chem.* **1990**, *19*, 301.
(8) Stigter, D.; Dill, K. A. *Biochemistry* **1990**, *29*, 1262.
(9) Warshel, A.; Chu, Z. T.; Parson, W. W. *Science* **1989**, *246*, 112.
(10) Russell, A. J.; Fersht, A. R. *Nature* **1987**, *328*, 496.
(11) Varadarajan, R.; Lambright, D. G.; Boxer, S. G. *Biochemistry* **1989**, *28*, 3771.
(12) Varadarajan, R.; Zewert, T. E.; Gray, H. B.; Boxer, S. G. *Science* **1989**, *243*, 69.
(13) Ware, W. R.; Lee, S. K.; Brant, G. J.; Chow, P. P. *J. Chem. Phys.* **1971**, *54*, 4729.
(14) DeToma, R. P.; Easter, J. H.; Brand, L. *J. Am. Chem. Soc.* **1976**, *98*, 5001.
(15) DeToma, R. P.; Brand, L. *Chem. Phys. Lett.* **1977**, *47*(2), 231.
(16) Halliday, L. A.; Topp, M. R. *Chem. Phys. Lett.* **1977**, *48*, 40.
(17) Shapiro, S. L.; Winn, K. R. *Chem. Phys. Lett.* **1980**, *71*, 440.
(18) Okamura, T.; Sumitani, M.; Yoshihara, K. *Chem. Phys. Lett.* **1983**, *94*, 339.

(19) Flom, S. R.; Nagarajan, V.; Barbara, P. F. *J. Phys. Chem.* **1986**, *90*, 2085.
(20) Brearly, A. M.; Flom, S. R.; Nagarajan, V.; Barbara, P. F. *J. Phys. Chem.* **1986**, *90*, 2092.
(21) Castner, E. W. Jr.; Maroncelli, M.; Fleming, G. R. *J. Chem. Phys.* **1987**, *86*, 1090.
(22) Maroncelli, M.; Fleming, G. R. *J. Chem. Phys.* **1987**, *86*, 6221.
(23) Kahlow, M. A.; Kang, T. J.; Barbara, P. F. *J. Phys. Chem.* **1987**, *91*, 6452.
(24) Su, S.-G.; Simon, J. D. *J. Phys. Chem.* **1986**, *90*, 6475.
(25) Su, S.-G.; Simon, J. D. *Chem. Phys. Lett.* **1986**, *132*, 345.
(26) Simon, J. D.; Su, S.-G. *J. Chem. Phys.* **1987**, *87*, 7016.
(27) Simon, J. D.; Su, S.-G. *J. Phys. Chem.* **1988**, *92*, 2395.
(28) Macgregor, R. B.; Weber, G. *Nature* **1986**, *319*, 70.
(29) Abbreviations: Mb, myoglobin; apoMb, apomyoglobin; DANCA, 2-(*N,N*-dimethylamino-6-naphthoyl-4-*trans*-cyclohexanoic acid; TNS, *N*-(*p*-tolyl)-2-aminonaphthalene-6-sulfonate; NMR, nuclear magnetic resonance spectroscopy.
(30) Stryer, L. *J. Mol. Biol.* **1965**, *13*, 482.
(31) Gafni, A.; DeToma, R. P.; Manrow, R. W.; Braned, L. *Biophys. J.* **1977**, *17*, 155.
(32) Gratton, E.; Lakowicz, J. R. In *Structure and Motion: Membranes, Nucleic Acids, Proteins*; Clementi, E., Ed.; Adenine Press: Guilderland, NY, 1985; p 155.
(33) Bismuto, E.; Irace, G.; Colonna, G.; Jameson, D. M.; Gratton, E. *Biochem. Biophys. Acta* **1987**, *913*(2), 150.
(34) Bismuto, E.; Jameson, D. M.; Gratton, E. *J. Am. Chem. Soc.* **1987**, *109*, 2354.
(35) Ilich, P.; Prendergast, F. G. *J. Phys. Chem.* **1989**, *93*, 4441, and unpublished data from this laboratory.
(36) It is possible that the creation of the excited-state dipole is coupled to nuclear rearrangements, namely rotation about the bond between the N atom and the naphthalene ring (Doduik, H.; Kanety, H.; Kosower, E. M. *J. Phys. Chem.* **1979**, *83*, 515. Rullière, C.; Grabowski, Z. R.; Dobkowski, J. *Chem. Phys. Lett.* **1987**, *137*(5), 408). If true, the observed dynamics may, in part, reflect this motion. This system should suffer from this problem to a smaller degree than others which have been studied, as the volume swept out by rotation of a dimethyamino group by 90° is much smaller than that for an arylamine. Direct characterization of the dipole moment changes on absorption and emission using electric field effects is in progress in this laboratory, and preliminary results indicate similar dipole moment changes for absorption and fluorescence.
(37) Decatur, S.; Pierce, D. W.; Boxer, S. G. Unpublished results.
(38) Bashkin, J. S.; McLendon, G.; Mukamel, S.; Marohn, J. *J. Phys. Chem.* **1990**, *94*, 4757.
(39) Teale, F. W. *J. Biochim. Biophys.* **1959**, *35*, 543.
(40) Weber, G. Personal communication.
(41) Griko, Y. V.; Privalov, P. L.; Venyanimov, S. Y. *J. Mol. Biol.* **1988**, *202*, 127.
(42) Bouchy, M. In *Deconvolution and Reconvolution of Analytical Signals: Application to Fluorescence Spectroscopy*; Bouchy, M., Ed.; Institut National Polytechnique de Lorraine, Ecole Nationale Superieure des Industries Chimiques, Societe de Chemie-Physique de France: Nancy, France, 1982.
(43) The function as it appears in ref 22 contains a typographical error.
(44) Agmon, N. *J. Phys. Chem.* **1990**, *94*, 2959.
(45) Maroncelli, M.; Fee, R. S.; Chapman, C. F.; Fleming, G. R. *J. Phys. Chem.* **1991**, *95*, 1012.
(46) It is unclear whether dielectric relaxation has ever really been observed before in proteins. The absence of a clear demonstration of time-dependent Stokes shifts in tryptophan fluorescence which could not be interpreted in terms of population heterogeneity (Gratton, E., personal communication) has been especially problematic, as tryptophan can be found in a wide variety of environments in proteins, and its static emission spectrum is routinely interpreted in terms of solvent polarity. However, this situation may reflect the properties of the probe more than the properties of proteins. It is possible that the solvent polarity affects the relative emission intensities of the two low-lying excited states of indole, which is a fundamentally different mechanism than dielectric relaxation for producing solvent-dependent wavelength shifts. This question can be addressed independently by studying the absorption and emission properties of tryptophan in applied electric fields, which is in progress.
(47) Hofrichter, J.; Sommer, J. H.; Deutsch, R.; Ikeda-Saito, M.; Yonetani, T.; Eaton, W. A. *Biochemistry* **1985**, *24*, 2667.
(48) Treutlein, H.; Schulten, K.; Deisenhofer, J.; Michel, H.; Bruenger, A.; Karplus, M. In *The Photosynthetic Bacterial Reaction Center*; Breton, J., Verméglio, A., Eds.; Plenum Press: New York, 1988; p 139.
(49) Treutlein, N.; Schulten, K.; Niedermeier, C.; Deisenhofer, J.; Michel, H.; DeVault, D. In *The Photosynthetic Bacterial Reaction Center*; Breton, J., Verméglio, A., Eds.; Plenum Press: New York, 1988; p 369.
(50) Treutlein, H.; Schulten, K.; Bruenger, A. T.; Karplus, M.; Deisenhofer, J.; Michel, H. *Proc. Natl. Acad. Sci. U.S.A.* **1992**, *89*, 75–59.
(51) Steinbach, P. J.; Ansari, A.; Berendzen, J.; Braunstien, D.; Chu, K.; Cowen, B.; Ehrenstein, D.; Frauenfelder, H.; Johnson, J. B.; Lamb, D. C.; Luck, S.; Mourant, J. R.; Nienhaus, G. U.; Ormos, P.; Phillip, R.; Xie, A.; Young, R. D. *Biochemistry* **1991**, *30*, 3988.
(52) Chen, Y.-M.; Pearlstein, A. J. *Ind. Eng. Chem. Res.* **1987**, *26*, 1670.
(53) Balasubramanian, S.; Lambright, D. G.; Boxer, S. G. Unpublished results.
(54) van der Zwan, G.; Hynes, J. T. *J. Phys. Chem.* **1985**, *89*, 4181.
(55) Livesey, A. K.; Brochon, J. C. *Biophys. J.* **1987**, *52*, 693.
(56) Gull, S. F.; Daniel, G. J. *Nature* **1978**, *272*, 686.
(57) Skilling, J.; Bryan, R. K. *Mon. Not. R. Astron. Soc.* **1984**, *211*, 111.
(58) Hirono, S.; Kollman, P. A. *Protein Eng.* **1991**, *4*(3), 233.
(59) Demchenko, A. P. *Biophys. Chem.* **1982**, *15*, 101–109.
(60) Demchenko, A. P. *Eur. Biophys. J.* **1988**, *16*, 121–129.
(61) Rosenthal, S. J.; Xie, Xiaoliang; Du, M.; Fleming, G. R. J. *Chem. Phys.* **1991**, *95*(6), 4715–4718.